RSC Advances

ROYAL SOCIETY OF CHEMISTRY

www.rsc.org/advances

Cite this: DOI: 10.1039/c0xx00000x

www.rsc.org/xxxxxx

COMMUNICATION

Solvent sensors based on amorphous ZnSnO thin-film transistors

Q. J. Jiang,[a]C. J. Wu,[a]J. P. Cheng,[a]X. D. Li,[b]B. Lu,[a]Z. Z. Ye,[a]J. G. Lu* [a]

Received (in XXX, XXX) XthXXXXXXXXX 20XX, Accepted Xth XXXXXXXXX 20XX
DOI: 10.1039/b000000x

Amorphous zinc-tin oxide (*a*-ZTO) thin-film transistors (TFTs) were prepared using a combustion solution method. The properties of *a*-ZTO films and *a*-ZTO TFTs were studied in detail. For applications, *a*-ZTO TFTs are used as solvent sensors. The *a*-ZTO TFTs exhibited strong sensitivity and selectivity in detecting solvents (e.g., cyclohexane, ethanol, and deionized water). The electron donors into the ZTO channels were determinated by the polarity of the solvent, which affects the location of Femi level (E_f). Moreover, a feasible mechanism model related to electron transfer channel (ETC) was proposed to explain the sensor behaviours. This model can be applied to most of the amorphous oxide TFT sensors. This work is expected not only to provide an insight into the fundamental understanding of behaviours of amorphous oxide TFT biosensors, but also to offer a basic design guideline for device fabrication in this system.

Recently, amorphous oxide semiconductor (AOS) thin-film transistors (TFTs) have attracted great interest for flat panel and next-generation displays.[1-7] In particular, ZnInO (ZIO) based AOSs have been extensively investigated in past years.[8,9] The full-scale production of displays using InGaZnO TFTs has been carried out in manufacturers.[10-13] However, the toxicity, limited storage, and high cost of In prevent the long-term application in all the fields. Therefore, indium-free AOSs are urgently pursued to meet the requirements. Amorphous ZnSnO (*a*-ZTO) emerges as one of the most promising indium-free alternatives, which has received more and more attention.[14,15]

More recently, several reports have appeared for DNA detections using ZIO-based TFT biosensors.[13] These reports promote the developments of oxide TFT sensors for detecting DNA, enzyme, and organic solvents. Unlike the traditional fluorescence techniques, TFT sensor is a "label-free" method, yielding many advantages such as high sensitivity and direct transduction.[14] Furthermore, small-sized and high-density TFT arrays have an intuitive appeal as portable or packed-sized sensors at low cost, which will benefit the developments of a device platform for the direct and rapid medical diagnosis.[15] Therefore, AOS TFT-based sensors exhibit a broad range of applications and potentially lower manufacturing costs.[16,17]

[a]*State Key Laboratory of Silicon Materials,School of Materials Science and Engineering, Zhejiang University, Hangzhou 310027, China.*
E-mail:lujianguo@zju.edu.cn;
[b]*Xinyi PV Products (Anhui) Holdings LTD., Xinyi PV Glass Industrial Zone, No. 2 Xinyi Road, ETDZ,Wuhu 241009, China*

In this communication, we develop new solvent sensors using *a*-ZTO TFTs. Based on a sole trigger, the electrostatic force between the targets and the detection area, *a*-ZTO based TFTs are effective to detect organic solvents including H_2O. Moreover, ZTO may be a favourable AOS for immobilization of biomolecules with low isoelectric points such as DNA through electrostatic interaction without any electron mediator. In our work, a combustion solution process is carried out to fabricate *a*-ZTO TFTs and the TFTs are used to detect different solvents (e.g., cyclohexane, ethanol, and deionized water) with high reliability and practicality. A feasible mechanism model related to electron transfer channel (ETC) is proposed to explain the sensor behaviours.

For *a*-ZTO precursors, solutions (Zn:Sn = 4:7 in molar ratio) were achieved by mixing the individual precursor and aging for 24 h. Individual precursors were synthesized by dissolving $SnCl_2$ with NH_4NO_3 or $Zn(NO_3)_2$ in 2-methoxyethanol, acetylacetone, and NH_3 (14.5 M) solutions, respectively. Then, *a*-ZTO channel films were prepared with a combustion process by spin-coating the precursors on 150 nm SiO_2/n^{++} Si wafers (University Wafer) at 4300 r.p.m. for 35 s, followed by an annealing process at 300 ºC for 30 min under air. To obtain the desired thickness, the above steps were repeated for several times. Al metal was employed for the source and drain electrodes by an electron beam evaporation technology. The resultant channel width and length were 1000 and 100 um, respectively. The pure solvents (cyclohexane, ethanol, and deionized water) were dropped onto the exposed *a*-ZTO channel surface with a micropipette, and the devices were then set in ambient air to evaporate the solvents for detections.

The crystal phase identification was investigated by an X-ray diffraction (XRD, Bede D1) system with Cu *Ka* radiation (λ= 0.15406 nm) over the 2θ range of 10-90°. Cross-section microstructure and element line sweeping were carried out using high-resolution transmission electron microscopy (HRTEM, TecnaiG2F20 S-Twin). Thermogravimetric analysis (TGA) and differential thermal analysis (DTA) were carried out by TA Q600 under a N_2 atmosphere at 5 ºC min^{-1} in the temperature range of 25 ºC-400 ºC. X-ray photoelectron spectroscopy (XPS, Thermo ESCALAB 250) measurements were performed to investigate the chemical bonding states with a monochromatic Al-Ka (1486.6 eV) X-ray source. Moreover, the signal responses of these biosensors were measured at RT in the dark using an Agilent E5270B.

Fig. 1(a) shows the XRD pattern of the ZTO film. The

prepared film is amorphous because there is no obvious

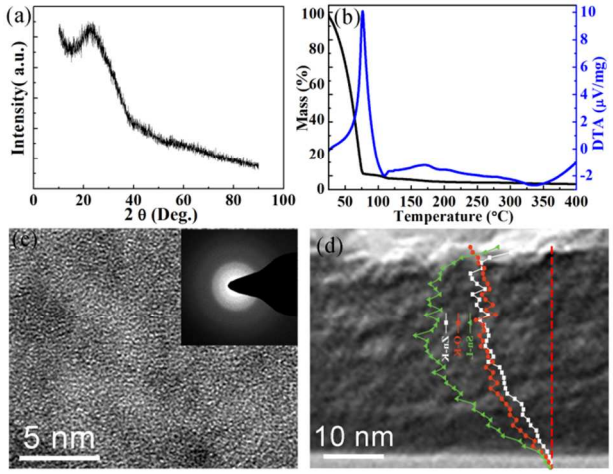

Fig. 1 (a) XRD patterns of *a*-ZTO films, (b) TGA and DTA of ZTO precursors, (c) HR-TEM and SAED images of *a*-ZTO films, and (d) cross-section HR-TEM and EDX line profiles of *a*-ZTO films.

diffraction peak of the crystalline phase. The halo peak around 23° is attributed to the glass substrates.[2,6] Fig. 1(b) depicts the TGA and DTA of ZTO precursors. The ZTO DTA reveals a sharp, intense exotherm at about 80 ºC, corresponding to the onset of combustion and corresponding abrupt and gradual mass losses. The self-energy generating combustion chemistry makes a crucial role in driving the reaction, thus completing the whole film fabrication.[18] The low decomposition temperature enables flexible sensors possible. Figs. 1(c) and 1(d) display the HR-TEM image, selected area electron diffraction (SAED) pattern, and cross-section HR-TEM image with energy dispersive x-ray (EDX) line profiles of the ZTO film. As shown in the images, the prepared film is indeed amorphous phase without Zn or Sn related aggregation or lattice-ordered groups.[6,19] From the cross-sectional HR-TEM, the film is dense and with a thickness of about 35 nm. The EDX profile also indicates that the Zn, Sn and O elements distribute uniformly along the cross-sectional film. The relative peak intensity of Zn-K and Sn-L reveals that the molar ratio of Zn to Sn is approximately 4:(5~8) in the matrix, which fits well with that in the solution.

XPS measurements have been carried out to investigate the Zn, Sn and O chemical bonding states. During the analysis, all the binding energy data are calibrated by taking C 1s reference at 284.8 eV to compensate for any charge-induced shifts. Figs. 2 (a) and 2 (b) show the Zn $2p_{3/2}$ and Sn $3d_{5/2}$ XPS spectra of the *a*-ZTO film, which are located at about 1021.9 and 486.7 eV, respectively, indicating the characteristic values of fully oxides.[20] Fig. 2 (c) depicts the O 1s XPS spectrum of the *a*-ZTO film. By using the Gaussian curve approximation, the typical O 1s peak is deconvoluted into three binding peaks: (1) O_I, M-O-M lattice species at 530.4 eV, (2) O_{II}, oxygen-deficient regions at 531.6 eV, and (3) O_{III}, weakly bound (M-OR) species such as H_2O, O_2, -OH and -CO_3 at 532.3 eV.[21] In general, the O_{II} peak area is

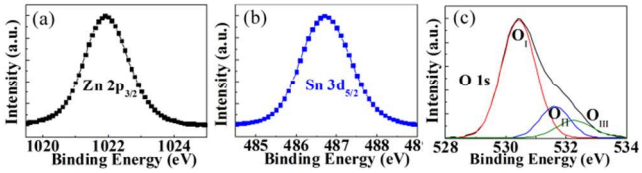

Fig. 2 (a) Zn $2p_{3/2}$, (b) Sn $3d_{5/2}$, (c) O 1s XPS spectra of *a*-ZTO film.

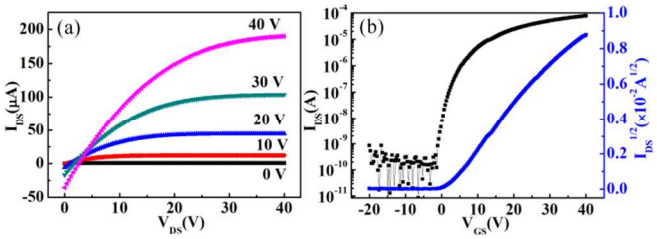

Fig. 3 (a) output and (b) transfer characteristics of a typical *a*-ZTO TFT.

proportional to the oxygen vacancy (Vo) concentration,[20] so the ratio of S_{OII}/S_{all} is used to obtain a relative Vo concentration in the *a*-ZTO film, where S_{OII} represents the integral area of O_{II} peak and S_{all} is the total area of the three peaks. Here, a ratio of 16.37% is obtained, indicating an appropriate value.[22]

Figs. 3 depicts the typical output and transfer characteristics of *a*-ZTO TFTs. The field effect mobility (μ_{FE}) and the threshold voltage (V_{th}) are deduced from the following equation,

$$I_{DS}^{1/2} = \sqrt{\frac{W}{2L} C_i \mu_{FE} (V_{GS} - V_{th})} \qquad V_{DS} \geq V_{GS} - V_{th} \tag{1}$$

where I_{DS}, V_{DS}, V_{GS}, C_i, W, and L are the drain current, drain-source voltage, gate bias, capacitance per unit area of the gate insulator (0.023 μF/cm^2), channel width, and channel length, respectively. The subthreshold swing (*SS*), a significant parameter to indicate the interface trap density, is calculated by

$$SS = \left(\frac{d \log(I_{DS})}{dV_{GS}} \right)^{-1} \tag{2}$$

The density of the interfacial trap states (N_t) at the ZTO channel/SiO_2 interface can be determined using the following equations,[22]

$$N_t = \left[\frac{SS \log(e)}{(kT/q)} - 1 \right] \frac{C_i}{q} \tag{3}$$

where *e*, *K*, *T*, and *q* are the Euler's constant, Boltzmann constant, temperature and quantity of one electron, respectively. For our *a*-ZTO TFTs, the device behaviours are I_{on}/I_{off}=10^5–10^6 with a low off-current in an order of about 10^{-11} A, μ_{FE}=1–3 cm^{2}V^{-1}S^{-1}, and V_{th}=-1–2 V. In what follows the TFTs are used to detect the solvents. In every detection case, three TFT devices were applied and the changes of the transfer characteristics for every solvent are almost the same.

The solvent sensors based on *a*-ZTO TFTs are demonstrated using nonpolar cyclohexane and polar C_2H_5OH and H_2O as the solvents, and the corresponding I_{DS}–V_{GS} characteristics are shown in Fig. 4. For nonpolar cyclohexane (Fig. 4(a)), there is little change of I_{on}/I_{off} (in the 3.11×10^5–3.21×10^5 range) and V_{th} (in the 0.35–0.53 range) after immobilizing cyclohexane for aging time of 0 and 360 min. This phenomenon indicates the TFT detector is not sensitive to this nonpolar solvent. While for polar C_2H_5OH(Fig. 4(b)), the I_{on}/I_{off} value decreases from 6.62×10^5 to 2.42×10^5 after immobilization (0 min), accompanied with the

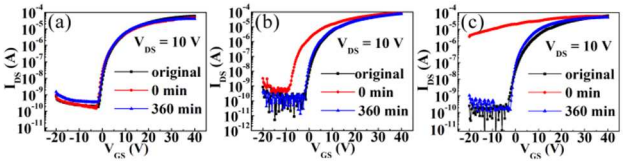

Fig. 4 Transfer characteristics of *a*-ZTO TFTs as solvent sensors for

Table 1 Electrical parameters (I_{on}/I_{off}, V_{th}, SS, and N_t) of *a*-ZTO TFT sensors for detecting different solvents.

	Cyclohexane			C_2H_5OH			H_2O		
Sample	original	0 min	360 min	original	0 min	360 min	original	0 min	360 min
I_{on}/I_{off} ($\times 10^5$)	3.21	3.21	3.11	6.62	2.42	5.05	5.45	—	3.46
V_{th}(V)	0.35	0.53	0.37	0.98	-5.49	1.22	-0.27	—	-0.70
SS(V/decade)	0.89	0.87	0.93	0.35	1.09	0.46	0.25	—	0.70
N_t($\times 10^{12}$ cm^{-2})	2.01	1.98	2.11	0.72	2.52	0.98	0.47	—	1.57

detecting solvents: (a) cyclohexane, (b) C_2H_5OH, and (c) H_2O.

a-ZTO TFT sensors in detecting different solvents: (a) cyclohexane, (b) C_2H_5OH, and (c) H_2O.

negative V_{th} shift from 0.98 V to -5.49 V. After aging 360 min under air, the electrical responses of the solvent sensor are I_{on}/I_{off} = 5.05×10^5 and V_{th}= 1.22 V, recovering to the original state. However, for strong polarity H_2O (18.26 MΩ) (Fig. 4(c)), the TFT loses the transfer characteristic with the I_{DS} value of 10^{-4}–10^{-5} A after immobilization (0 min). After 360 min, the device displays an I_{on}/I_{off} of 3.46×10^5 and V_{th} of -0.70 V, also recovering to the original state. Detailed value changes can be seen in Table 1. It is obvious seen that the *a*-ZTO TFT sensors are very sensitive to different solvents and exhibit a good selectivity. Notably, since the *a*-ZTO TFT sensors can recover to the original state after durations, they can be used repeatedly in practical applications. In general, electron injections from the channel surface or the channel matrix to the electron transfer channel (ETC) at the interface contribute to the changes of electrical properties.[23,24] It is expected that this effect can also be applied in our case. The detailed sensing mechanism schematics of *a*-ZTO TFTs to the various solvents (cyclohexane, C_2H_5OH and H_2O) are shown in Fig. 5. In AOS TFTs, the AOS film contains some shallow levels above the Femi level (E_f) but below the bottom of conduction band (E_c), which act as electron trapping centres.[25,26] At $V_{DS}\geq V_{GS}$-V_{th}, the energy band of the AOS channel bends to the channel/insulator interface due to the induced field (E). The electrons tend to accumulate at the channel/insulator interface, thus forming the ETC, and the E_f near the interface moves above onto the shallow trapping state level.[25] Meanwhile, the shallow trapping levels are all filled with electrons, which are captured from the channel during the applied bias. After immobilizing with cyclohexane on the *a*-ZTO back-channel, no extra electrons are injected into the channel due to the nonpolarity nature determined by the small dielectric constant (2.10). Generally, the larger dielectric constant corresponds to the stronger polarity. Therefore, amounts of accumulated electrons near the channel/insulator

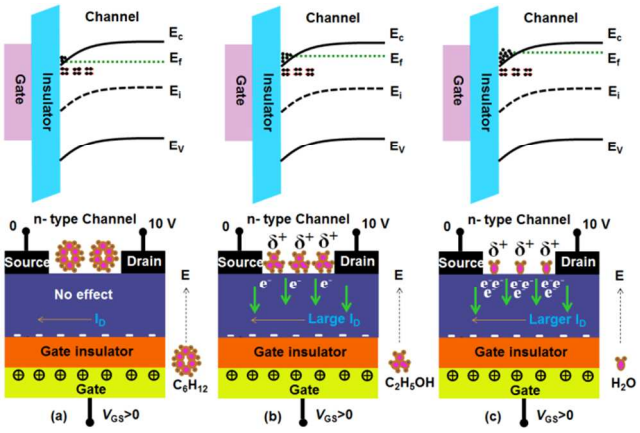

Fig. 5 Schematic diagram of mechanism model to explain behaviours of

interface are not changed. The shallow trapping levels and E_f keep original, as Fig. 5(a) displays. After aging for 0 and 360 min, the transfer characteristics do not change. The small SS and N_t changes (from original to 360 min) also indicate this phenomenon, as shown in Table 1. However, using strong polarity liquids like absolute alcohol (dielectric constant of 24.5), the C_2H_5OH molecules cause "donor effects" on the channel through the electron-donating hydroxyl group,[27]

$$C_2H_5OH = C_2H_5OH^+ + e \quad (4)$$

extra electrons are injected into the channel and accumulate at the interface, as shown in Fig. 5 (b). The E_f further moves above onto the shallow trapping state level and close to the E_c through the doping. While the shallow trapping levels are still filled with electrons. By the solvent donor effects, the V_{th} exhibits an evident negative shift with increased I_{DS} (Fig. 5(b)), which is consistent well with this proposed mechanism. The SS (from 0.35 to 1.09 V/decade) and N_t (from 7.20×10^{11} to 2.52×10^{12}) changes also indicate that the interface trap states are indeed increased by the injected electrons. After aging 360 min, the TFT sensor recovers to the original state (shown in Table 1). Naturally, using the strong polar solvent H_2O (dielectric constant of 78.5), it is quite reasonable to suppose that more extra electrons are generated into the ETC,[28-30]

$$H_2O = H_2O^+ + e \quad (5)$$

The massive electron injection induces the fact that the E_f tends much closer to the E_c, accompanied with fully filled electrons at the shallow defect levels, as Fig. 5(c) displays. Thus, the large I_{DS} is obtained and so as to make the TFT lose the transfer characteristic at 0 min (Fig. 4(c)). After aging 360 min, the sensor performance also recovers to the original state in the main. The analysis can be confirmed by the SS and N_t values, as listed in Table 1. Note that our recent study reveals that the *a*-ZTO TFT can be used to detect such biomaterials as DNA and enzyme, which will be reported elsewhere. The model presented here is also applied to these biosensor behaviours.

In summary, solvent sensors based on *a*-ZTO TFTs have been successfully demonstrated. The *a*-ZTO TFTs were fabricated using a combustion process and displayed a strong sensitivity in detecting solvents (e.g., cyclohexane, ethanol, and deionized water) with a good selectivity. A feasible mechanism model was developed to explain the sensor behaviours. The donor effects by the solvents determinate the location of Femi level (E_f), thus making the TFT different response. It is a reasonable and feasible model not only for our TFT detections, but also can be applied to other amorphous TFT detections.

This work was supported by National Natural Science Foundation of China under Grant no. 51372002 and Municipal Science &Technology Project of Wuhu City under Grant no.

2013zd18.

Notes and references

1 T. H. Chao, M. J. Chang, M. Watanabe, M. H. Luo, Y. J. Chang, T. C. Fang, K. Y. Chen and T. J. Chow, *Chem. Commun.*, 2012, **48**, 6148.

2 Q. J. Jiang, L. S. Feng, C. J. Wu, R. J. Sun, X. F. Li, B. Lu, Z. Z. Ye and J. G. Lu, *Appl. Phys. Lett.*, 2015, **106**, 053503.

3 M. G. Kim, M. G. Kanatzidis, A. Facchetti and T. J. Marks, *Nat. Mater.*, 2011, **10**, 382.

4 K. Nomura, H. Ohta, A. Takagi, T. Kamiya, M. Hirano and H. Hosono, *Nature*, 2004, **432**, 488.

5 C. J. Wu, X. F. Li, J. G. Lu, Z. Z. Ye, J. Zhang, T. T. Zhou, R. J. Sun, L. X. Chen, B. Lu and X. H. Pan, *Appl. Phys. Lett.*, 2013, **103**, 082109.

6 Q. J. Jiang, J. G. Lu, J. P. Cheng, X. F. Li, R. J. Sun, L. S. Feng, W. Dai, W. C. Yan and Z. Z. Ye, *Appl. Phys. Lett.*, 2014, **105**, 132105.

7 Y. P. Wang, J. G. Lu, X. Bie, Z. Z. Ye, X. Li, D. Song, X. Y. Zhao, and W. Y. Ye, *Appl. Surf. Sci.*, 2011, **257**, 5966.

8 J. W. Hennek, J. Smith, A. Yan, M. G. Kim, W. Zhao, V. P. Dravid, A. Facchetti and T. J. Marks, *J. Am. Chem. Soc.*, 2013, **135**, 10729.

9 H. W. Zan, C. C. Yeh, H. F. Meng, C. C. Tsai and L. H. Chen, *Adv. Mater.*, 2012, **24**, 3509.

10 W. B. Jackson, R. L. Hoffman and G. S. Herman, *Appl. Phys. Lett.*, 2005, **87**, 193503.

11 H. Q. Chiang, J. F. Wager, R. L. Hoffman, J. Jeong and D. A. Keszler, *Appl. Phys. Lett.*, 2005, **86**, 013503.

12 K. H. Lim, K. Kim, S. Kim, S. Y. Park, H. Kim and Y. S. Kim, *Adv. Mater.*, 2013, **25**, 2994.

13 Y. C. Shen, C. H. Yang, S. W. Chen, S. H. Wu, T. L. Yang and J. J. Huang, *Biosens.Bioelectron.*, 2014, **54**, 306.

14 F. Yan, S. M. Mok, J. Yu, H. L. Chan and M. Yang, *Biosens.Bioelectron.*, 2009, **24**, 1241.

15 S. J. Kim, J. Jung, K. W. Lee, D. H. Yoon, T. S. Jung, S. R. Dugasani, S. H. Park and H. J. Kim, *ACS Appl. Mater. Interfaces*, 2013, **5**, 10715.

16 S. J. Kim, B. Kim, J. Jung, D. H. Yoon, J. Lee, S. H. Park and H. J. Kim, *Appl. Phys. Lett.*, 2012, **100**, 103702.

17 J. Jung, S. J. Kim, K. W. Lee, D. H. Yoon, Y. G. Kim, H. Y. Kwak, S. R. Dugasani, S. H. Park and H. J. Kim, *Biosens.Bioelectron.*, 2014, **55**, 99.

18 M. G. Kim, M. G. Kanatzidis, A. Facchetti, and T. J. Marks, *Nat. Mater.,*2011,**10**, 382.

19 M. Kim, J. H. Jeong, H. J. Lee, T. K. Ahn, H. S. Shin, J. S. Park, J. K Jeong, Y. G. Mo,and H. D. Kim*, Appl. Phys. Lett.*, 2007, 9**0**, 212114.

20 M. G. Kim, H. S. Kim, Y. G. Ha, J. Q. He, M. G. Kanatzidis, A. Facchetti and T. J. Marks, *J. Am. Chem. Soc.*, 2010, **132**, 10352.

21 M. G. Kim, J. W. Hennek, H. S. Kim, M. G. Kanatzidis, A. Facchetti and T. J. Marks, *J. Am. Chem. Soc.*, 2012, **134**, 11583.

22 Y. S. Rim, D. L. Kim, W. H. Jeong and H. J. Kim, *Appl. Phys. Lett.*, 2010, **97**, 233502.

23 E. Fortunato, P. Barquinha and R. Martins, *Adv. Mater.*, 2012, **24**, 2945.

24 P. Wu, J. Zhang, J. G. Lu, X. F. Li, C. J. Wu, R. J. Sun, L. S. Feng, Q. J. Jiang, B. Lu, X. H. Pan and Z. Z. Ye, *IEEE T. Electron. Dev.*, 2014, **61**, 1431.

25 M. Kimura, T. Nakanishi, K. Nomura, T. Kamiya and H. Hosono, *Appl. Phys. Lett.*, 2008, **92**, 133512.

26 J. Zhang, X. F. Li, J. G. Lu, Z. Z. Ye, L. Gong, P. Wu, J. Huang, Y. Z. Zhang, L. X. Chen and B. H. Zhao, *J. Appl. Phys.*, 2011, **110**, 084509.

27 X. Y. Xue, Y. J. Chen, Y. G. Wang and T. H. Wang, *Appl. Phys. Lett.*, 2005, **86**, 233101.

28 J. K. Jeong, H. W. Yang, J. H. Jeong, M. Y. G. and K. H. D., *Appl.* Phys. *Lett.*, 2008, **93**, 123508.

29 J.S. Park, J. K. Jeong, H.J. Chung, Y.G. Mo and H. D. Kim, *Appl. Phys. Lett.*, 2008, **92**, 072104.

30 J. Zhang, X. F. Li, J. G. Lu, N. J. Zhou, P. J. Guo, B. Lu, X. H. Pan, L. X. Chen and Z. Z. Ye, *RSC Adv.*, 2014, **4**, 3145.